EPJ manuscript No.
(will be inserted by the editor)

Simulations of Kinetic Electrostatic Electron Nonlinear (KEEN) Waves with Two-Grid, Variable Velocity Resolution and High-Order Time-Splitting

B. Afeyan[1], F. Casas[2], N. Crouseilles[3], A. Dodhy[4], E. Faou[3], M. Mehrenberger[4,5], E. Sonnendrücker[4,6 a b]

[1] Polymath Research Inc., 827 Bonde Court, Pleasanton, CA 94566
[2] IMAC, Departament de Matemàtiques, Universitat Jaume I, 12071-Castellón, Spain
[3] Inria-Rennes (IPSO team) and IRMAR, Rennes, France
[4] Max-Planck-Institut für Plasmaphysik, Garching, Germany
[5] IRMA, Université de Strasbourg, France
[6] Mathematics center, TU Munich, Garching, Germany

Received: date / Revised version: date

Abstract. KEEN waves are nonlinear, non-stationary, self-organized asymptotic states in Vlasov plasmas outside the scope or purview of linear theory constructs such as electron plasma waves or ion acoustic waves. Nonlinear stationary mode theories such as those leading to BGK modes also do not apply. The range in velocity that is strongly perturbed by KEEN waves depends on the amplitude and duration of the ponderomotive force used to drive them. Smaller amplitude drives create highly localized structures attempting to coalesce into KEEN waves. These cases have much more chaotic and intricate time histories than strongly driven ones. The narrow range in which one must maintain adequate velocity resolution in the weakly driven cases challenges fixed grid numerical schemes. What is missing there is the capability of resolving locally in velocity while maintaining a coarse grid outside the highly perturbed region of phase space. We here report on a new Semi-Lagrangian Vlasov-Poisson solver based on conservative non-uniform cubic splines in velocity that tackles this problem head on. An additional feature of our approach is the use of a new high-order time-splitting scheme which allows much longer simulations per computational effort. This is needed for low amplitude runs which take a long time to set up KEEN waves, if they are able to do so at all. The new code's performance is compared to uniform grid simulations and the advantages quantified. The birth pains associated with KEEN waves which are weakly driven is captured in these simulations. These techniques allow the efficient simulation of KEEN waves in multiple dimensions which will be tackled next as well as generalizations to Vlasov-Maxwell codes which are essential to understanding the impact of KEEN waves in practice.

PACS. PACS-key 52.65.Ff Plasma simulation: Fokker-Planck and Vlasov equation

1 Introduction

Kinetic Electrostatic Electron Nonlinear (KEEN) Waves were discovered in 2002 while trying to decipher the validity of claims made about electron acoustic waves EAWs and their relationship to electron plasma waves (EPW) in the nonlinear, kinetic evolution of the Stimulated Raman Scattering (SRS) instability [14,15]. Since then, much work has been done to decipher the physics of KEEN waves. Unlike EPWs, or EAWs, KEEN waves do not exist on a dispersion curve predicted by an infinitesimal amplitude limit calculation where the distribution function has been assumed to be flat (with zero derivative) at the phase velocity of the wave. This assumption or generically imposed constraint ensures the existence of stationary structures for EPWs and EAWs. Instead, KEEN waves can be excited or driven by the ponderomotive force generated by the optical mixing of a pair of laser beams [1]. These two crossing laser beams drive a wave at their difference frequency and wavenumber. By changing the frequencies and wave numbers of the two laser beams in a given density and temperature plasma, we can drive KEEN waves anywhere in Brillouin (ω, k) space. Linear wave analysis of the Vlasov-Poisson system of equations, shows that for a

[a] A part of this work was carried out using the HELIOS supercomputer system at Computational Simulation Centre of International Fusion Energy Research Centre (IFERC-CSC), Aomori, Japan, under the Broader Approach collaboration between Euratom and Japan, implemented by Fusion for Energy and JAEA.
[b] BA would like to acknowledge the financial assistance of DOE OFES HEDP program through a subcontract via UCSD

Maxwellian plasma, for instance, resonant waves can only live on dispersion curves, which are familiar from plasma physics textbooks and are related to Landau's original work on Landau or collisionless damping of EPWs [11].

Outside these curves of measure zero in the (ω, k) plane, no (not heavily damped) waves were deemed possible, thus defining a spectral gap in plasma theory. But nonlinear stationary states were known to exist, referred to as BGK modes [4]. This is predicated on one's ability to cobble a distribution function in phase space that would accommodate such states. These stationary modes (in some Galilean frame of reference and constituting a function of the canonically conjugate variable to time, namely, energy) require strong distribution function modification. Thus, they beg the question of how they would come about starting with a Maxwellian. Or, whether some other states would predominate much before these stationary states were ever settled into. The discovery of KEEN waves [1] answers these questions in favor of the latter. Since KEEN waves can occur anywhere in the (ω, k) plane and not just on the EPW and EAW dispersion curves, KEEN waves remove the delicate nature of linear, resonant modes.

We now know that EAWs and BGK modes, which do have an infinitesimal amplitude limit, are not the only type of nonlinear structure to be expected in a time dependent setting. KEEN waves demonstrate that the requirement of stationarity can be dropped in favor of much richer structures and that non stationary, constantly evolving and adapting phase space structures are in fact ubiquitous. The basic physics is that a multi-harmonic phase-locked electric field structure is created, even though only one harmonic was driven, which can trap, untrap and retrap particles whose orbits are near the non-stationary separatrix. These lost particles are not retrapped exactly where they were lost but elsewhere in the troughs of the field after crossing many crests in either direction. This is the origin of the persistent non-stationarity. While KEEN waves are harder to excite and self-organize, they are very robust to perturbations while delicate resonant modes have the opposite property, namely, easy to excite but easily detuned or disturbed by perturbations.

The self-adjusting multi-harmonic field structure can trap enough of the particles to maintain itself in perpetuity within the Vlasov-Poisson or Vlasov-Maxwell [17] set of equations. With KEEN waves, deeply trapped particles remain trapped, but the separatrix regions harbor far more complicated dynamics. The weaker the drive, the more the entire fate of the mode is dictated by these separatrix regions. The stronger the drive, the deeper the wells and the less stringent is the loss mechanism on the overall sustainability of the mode. But as the drive is diminished, the dynamics becomes more complicated, chaos dominates and small vortices do not have the ability to merge and form a KEEN wave. The process takes longer and longer and may become disrupted by other physical processes such as collisions or side-losses which are not included in this $1D \times 1D$ Vlasov-Poisson model.

We have observed KEEN waves in the laboratory driven exactly as stated above, via the ponderomotive force emanating from the optical mixing of two laser beams. For details of those experiments conducted on the Trident laser system at Los Alamos, see [10].

Here we wish to study the transition region between a well formed KEEN wave and more fledgling scenarios by varying the drive time of the ponderomotive force, externally-imposed, and following the long time evolution of the structures that remain and persist long after the drive is turned off (and the system acquires a Hamiltonian nature). Two crucial new elements are introduced to make these studies possible. First a new code is used which does not use a fixed velocity grid Vlasov solver. Instead, a two grid system is adopted. Fine scale resolution is imposed within the region in velocity around the phase velocity of the driven wave where the vortical structures are formed, surrounded by a coarser scale external region. The external region reacts to KEEN waves by absorbing its wake and this must be computed correctly in order to gather the correct overall charge density to be used on the right hand side of the Poisson equation. The variable grid technique allows the relevant v-space region to shrink without requiring massive fine scale resolution throughout the entire velocity range. Just the perturbed region is finely resolved, no matter how small it gets. Secondly, since long time evolution is what is of most interest, it was desirable to have a way to speed up the calculations without losing accuracy, especially when faced with chaotic dynamics that has to be tracked with low amplitude drive. The mutual attraction and commingling of many vorticlets at low amplitude drive can cause one to question the accuracy and fidelity of low-order, long time simulations. The usual modern answer when facing such circumstances is to appeal to symplectic and higher order integration schemes. Clever tricks are deployed to simplify the higher order splitting tasks [6] which allow to implement a sixth order in time, operator splitting scheme.

Armed with these two new techniques, we have simulated weak drive amplitude KEEN wave generation with a sequence of drive durations that extend from no KEEN wave formation to healthy KEEN wave formation. Intuitively we know that it is the amount of energy that is directly coupled into the KEEN wave that will dictate its final size or strength. But the scaling with drive time is not linear. There is in fact a saturation of that directly driven mode that sets in. The driven mode at its maximum amplitude will collapse and channel its energy to higher order modes, starting with the second harmonic. This is repeated between the second and the third harmonics and so on. Meanwhile, the drive is shut off and the modes rearrange themselves and adjust to a trapped-untrapped and retrapped distribution of particles that restore energy back into the field the lower few harmonics that constitute the essential elements of a KEEN wave. An important question is how long must the drive be, for a certain amplitude drive, so that trapping sets in for large scale vortices that do not disintegrate after the drive is off but which can maintain the KEEN wave.

In this paper, we show a number of examples of KEEN wave generation and evolution and compare uniform ve-

locity grid simulations to multiple contiguous and variable grid simulations, with the added feature of an easy to implement sixth-order symplectic (split-step) integrator. We will show that by taking too large a time step, such as a a full plasma frequency inverse, errors do eventually accumulate and contaminate the simulations. In our work to date, we can not claim full convergence in Δx, Δv and Δt for long time simulations. But much more efficient simulations are now possible without the waste of fine scale resolution in velocity space in regions where there are no significant disturbances (far from the phase velocity of the driven KEEN wave). But full convergence in chaotic high dimensional dynamics is not strictly expected except in some statistical sense. More work will be done in this direction in the near future.

The $1D\times1D$ Vlasov-Poisson equation for $f = f(t, x, v)$ with an external driving electric field $E_{\rm app}$ reads:

$$\partial_t f + v\partial_x f + (E - E_{\rm app})\partial_v f = 0,\ \partial_x E = \int_{\mathbb{R}} f dv - 1.$$

Here $E_{\rm app}(t, x)$ is of the form

$$E_{\rm app}(t, x) = E_{\max} k a(t) \sin(kx - \omega t),$$

with

$$a(t) = \frac{g(t) - g(t_0)}{1 - g(t_0)},$$

$$g(t) = 0.5(\tanh(\frac{t - t_L}{t_{wL}}) - \tanh(\frac{t - t_R}{t_{wR}})),$$

$t_0 = 0$, $t_L = 69$, $t_{wL} = t_{wR} = 20$, $t_R = 207 + T_{\rm dr}$, $k = 0.26$, $\omega = 0.37$. The initial condition is

$$f_0(x, v) = \frac{1}{\sqrt{2\pi}} \exp\left(-\frac{v^2}{2}\right), \quad (x, v) \in [0, 2\pi/k] \times [-6, 6].$$

Two typical cases will be considered : the **standard drive**, with $T_{dr} = 100$ and $E_{\max} = 0.2$, and the **small drive**, with $T_{\rm dr} = 200$ and $E_{\max} = 0.00625$. Final time is fixed to $T = 1000$ in the standard case and $T = 5000$ in the small drive case. Then, we will show some numerical results, by varying the drive time $T_{\rm dr}$, for the small drive amplitude $E_{\max} = 0.00625$, in order to see the influence on the formation of KEEN waves.

The simulation of KEEN waves is quite challenging: such test case develops small localized structures at large final time, which typically requires a high number of phase space points and a small time step. Some recent works can be found in [7,13,18]. Here, we continue the work initiated in [13], where the standard case was simulated; there a classical semi-Lagrangian method with high order Lagrange interpolation, or splines, with Strang splitting was used. The influence of single/double precision was studied and a delta-f method was introduced in order to improve single precision results, which generally damage the numerical results in such a test problem. The use of GPU has permitted to run efficiently some quite refined simulations (grid 2048×2048 in double precision and 4096×4096 in double precision; time step until 0.01). However, as shown on the numerical results, we were not able to get late time convergence of the first Fourier modes of the charge density and the phase space plots look quite similar but can be shifted and present some differences depending on the numerical parameters that are used, at the final time. The aim of this present paper is to study some improvements of the semi-Lagrangian scheme [13] and to see the influence of different numerical parameters for the standard case, and also for a case of small drive amplitude. The simulations require a high resolution around the phase velocity of the drive wave, and this region becomes very small when the drive amplitude is small. A lot of runs have been done, by changing different numerical parameters. We try here to report some of the most significant ones. This should help designing in the future what numerical parameters should be used, and it is a first step, for a parametric study [3], which is here initiated, by looking at the influence of the duration of the drive in the small drive amplitude case. More elaborated physical diagnostics should also be added. In Section 2, we will detail the main ingredients of the numerical method, that is the conservative non uniform cubic splines reconstruction and the high order splitting in time. Section 3 is devoted to the numerical results: first two canonical cases will be discussed in detail, with small and standard amplitude drive; finally, numerical simulations will be reported, varying the drive time, for the small drive amplitude case.

2 Numerical method

Obtaining numerical convergence is quite hard, as we have here no exact solution. What we can do is to run simulations for different numerical parameters and then see if the simulations are approaching together as we refine the space/velocity/time grid. In order to succeed, up to a certain accuracy, in this task and to improve the former work [13], we have used mainly three ingredients. The first one, is the MPI parallelization of the code (previous versions were OPENMP or GPU) which is developed within the library Selalib [16], in order to improve the speed of the simulation; optimizations may be performed, in order to see what we could further gain. The second one is the use of non uniform conservative cubic splines, in order to be able to capture the vortices arising in a small region in velocity. The third one is the use of high order splitting in time [6], in order to be able to reduce the number of iterations, and to see the influence of the time discretization. In the sequel, we will detail the main features of the developed numerical methods.

2.1 The two-grid mesh in velocity

We have to generate a $1D$ velocity mesh that is fine in a small region and coarse elsewhere, as activity in the distribution function is located in a small region in velocity, depending on the drive amplitude. The strategy that is adopted here is to define a coarse grid which has a refined region. Such specific grid has the advantage of being very

simple; also specific numerical methods may be designed for such grids. Mesh spacing on coarse/fine grids are

$$\Delta v_{\text{coarse}} = \frac{v_{\max} - v_{\min}}{N_{\text{coarse}}},\ \Delta v_{\text{fine}} = \frac{v_{\max} - v_{\min}}{N_{\text{fine}}}$$

and N_{fine} is an integer multiple of N_{coarse}.
The refined zone is chosen with $0 \le i_1 < i_2 \le N_{\text{coarse}}$ and the total number of cells is

$$N = i_1 + N_f + N_{\text{coarse}} - i_2,\ N_f = \frac{N_{\text{fine}}}{N_{\text{coarse}}}(i_2 - i_1)$$

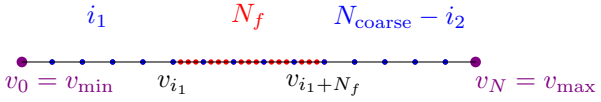

In order to generate such mesh, we have chosen as input parameters the total number of cells N, the region where we want to refine $v_{\min} \le a < b \le v_{\max}$ and an integer ratio $r \neq 1$. From these values, we look for

$$i_1,\ i_2,\ N_{\text{coarse}}$$

such that

$$v_{\mathrm{i_1}} \simeq a,\ v_{\mathrm{i_1+N_f}} \simeq b,\ r = \frac{N_{\text{fine}}}{N_{\text{coarse}}}.$$

For this, we detail the algorithm that we have chosen. We first write

$$\alpha = \frac{a - v_{\min}}{v_{\max} - v_{\min}},\ \beta = \frac{b - v_{\min}}{v_{\max} - v_{\min}}$$

and compute

$$N^*_{\text{coarse}} = \left\lfloor \frac{N}{1 + (\beta - \alpha)(r-1)} \right\rfloor,\ N_{\text{fine}} = r N^*_{\text{coarse}},$$

together with

$$i^*_1 = \lfloor \alpha N^*_{\text{coarse}} \rfloor,\ \ell = \left\lfloor \frac{N - N^*_{\text{coarse}}}{r-1} \right\rfloor,$$

in order to obtain

$$N_{\text{coarse}} = N - \ell(r-1),\ i_1 = \lfloor \alpha N_{\text{coarse}} \rfloor,\ i_2 = i_1 + \ell.$$

Other strategies may be studied or be more efficient; we could also try to change the grid in order to smooth the change of mesh spacing, which here goes directly from Δv_{coarse} to Δv_{fine}.

2.2 Conservative cubic splines on non uniform mesh

One popular semi-Lagrangian method for the numerical resolution of the Vlasov-Poisson equation is to use dimensional splitting [8] and cubic splines for the interpolation. Here the mesh in velocity is not uniform and we can deal with non uniform cubic splines. However, we lose the conservation of mass, when the mesh is non uniform and that seriously affects the numerical results in this typical test problems; see [13], where we see the effects of non conservation of mass due to the use of single precision computations. Thus, instead of looking at the classical advective form of the constant advection equation, we can consider the conservative form [9]. That means that we reconstruct the primitive function, using the same interpolation operator. We have to take care about the boundary conditions, that are here considered periodic, and we will have also to shift the unknowns to the middle of the velocity cells, in this non uniform setting (this is not necessary, for the uniform grid case). We now detail the different steps of the algorithm.
Thanks to dimensional splitting, we are lead to solve

$$\partial_t u + c\partial_v u = 0,$$

over a time step Δt (or fraction of time step, as we will see later), with unknowns

$$u_{j+1/2}(t) = \frac{1}{v_{j+1} - v_j} \int_{v_j}^{v_{j+1}} u(v,t)dv,\ j = 0, \ldots, N-1.$$

That is, we are supposed to know

$$u^{\text{old}}_{j+1/2} \simeq u_{j+1/2}(0),\ j = 0, \ldots, N-1,$$

and we want to compute

$$u^{\text{new}}_{j+1/2} \simeq u_{j+1/2}(\Delta t),\ j = 0, \ldots, N-1.$$

Using the conservation of the volume, we have the relation

$$\int_{v_j}^{v_{j+1}} u(v, \Delta t)dv = \int_{v_j - c\Delta t}^{v_{j+1} - c\Delta t} u(v,0)dv.$$

We first compute

$$U_j = \sum_{k=0}^{j-1} (u^{\text{old}}_{k+1/2} - M)(v_{k+1} - v_k),\ j = 0, \ldots, N,$$

with

$$M = \sum_{k=0}^{N-1} u^{\text{old}}_{k+1/2}(v_{k+1} - v_k).$$

Note that, by construction, we have $U_N = U_0 = 0$. We then define the non-uniform cubic spline interpolation of the primitive, that is the unique piecewise cubic polynomial function $U_h \in C^2_{\text{per}}(v_0, v_N)$ satisfying

$$U_h(v_j) = U_j,\ U_h \text{ polynomial on } [v_j, v_{j+1}],\ j = 0, \ldots, N-1.$$

This can be done classically by solving a system which is almost tridiagonal, for computing the spline coefficients or the Hermite derivatives; see e.g. [5]. Note that the primitive is periodic, thanks to the choice of the integration constant M. Finally, we compute

$$U^{\text{new}}_j = U_h(v_j - c\Delta t),\ j = 0, \ldots, N-1,$$

and get the unknowns updated by

$$u_{j+1/2}^{\text{new}} = \frac{U_{j+1}^{\text{new}} - U_j^{\text{new}}}{v_{j+1} - v_j} + M,\ j = 0, \ldots, N-1.$$

Note that the method is conservative by construction, as we get

$$\sum_{j=0}^{N-1} u_{j+1/2}^{\text{new}}(v_{j+1} - v_j) = M.$$

Other strategies can be envisaged, by using the special structure of the two-grid mesh [12], but are here not further developed.

2.3 High order time splitting

We fix a time step Δt and consider a list of coefficients $a_1, \ldots, a_s$, with $s \in \mathbb{N}^*$, together with a coefficient $\sigma_{\text{init}} \in \{0, 1\}$.
For $n \in \mathbb{N}$, we know

$$f_{i,j}^n \simeq f(n\Delta t, x_i, v_{j+1/2})$$

Index i will go from 0 to $N_x - 1$ and j from 0 to $N_v - 1$. We fix $t^* \to n\Delta t$ and $\sigma \to \sigma_{\text{init}}$, and start with $f_{i,j}^* \to f_{i,j}^n$. For each $k = 1, \ldots, s$, we make the $\mathcal{T}^\sigma$ advection over a time step $\Delta\tau \to a_k \Delta t$ and then update $\sigma \to 1 - \sigma$.
Here $\mathcal{T}^0$ (advection in x) consists in solving over a substep $\Delta\tau$

$$\partial_t f(t, \cdot, v_{j+1/2}) + v_j \partial_x f(t, \cdot, v_{j+1/2}) = 0,$$

to update $f_{i,j}^*$. At the end, we update $t^* \to t^* + a_k \Delta t$.
$\mathcal{T}^1$ (advection in v) consists in computing the electric field $E^*(x_i)$ via the Poisson equation (see e.g. [13]) and solve over a substep $\Delta\tau$

$$\partial_t f(t, x_i, \cdot) + (E^*(x_i) - E_{\text{app}}(t^*, x_i))\partial_v f(t, x_i, \cdot) = 0,$$

to update $f_{i,j}^*$. At the end of the substep s, we get $f_{i,j}^{n+1} \to f_{i,j}^*$.
Classical Strang splitting, that will be used here for comparison, corresponds to $s = 3,\ a_1 = 1/2,\ a_2 = 1,\ a_3 = 1/2$ and $\sigma_{\text{init}} = 1$.
We have developed new efficient high order schemes for Vlasov-Poisson, see [6], exploiting the specific structure of the Vlasov-Poisson system. The 6th order Vlasov-Poisson splitting scheme, that is used in the numerical results, has the following coefficients: $s = 11$,

$$\begin{aligned}
a_1 &= 0.04908646097611624549144 12 \\
&\quad -2\Delta t^2(0.00006972871505530508409 99), \\
a_2 &= 0.16873595056343742244819 57, \\
a_3 &= 0.26417760988897670020014 62 \\
&\quad -2\Delta t^2(0.00062570482743004718916 9) \\
&\quad +4\Delta t^4(-2.91660045768984781644 \cdot 10^{-6}), \\
a_4 &= 0.37785158922092830388076 6, \\
a_5 &= 0.18673592913490705430841 26 \\
&\quad -2\Delta t^2(0.00221308512404532556163) \\
&\quad +4\Delta t^4(0.00003048480261700038788 68) \\
&\quad -8\Delta t^6(4.98554938787506812159 \cdot 10^{-7}), \\
a_6 &= -0.09317507956873145265792 44,
\end{aligned}$$

together with $a_{6+i} = a_{6-i},\ i = 1, \ldots, 5$ and $\sigma_{\text{init}} = 1$.

3 Numerical results

In all the numerical results, we have used $v_{\max} = 6$, Lagrange interpolation of degree 17 in x (see [13]) and by default $N_x = 2048$. In the v-direction, we use cubic splines, that is conservative non uniform cubic splines; when the mesh is uniform, this corresponds to classical cubic splines; for the sake of simplicity, we have used the same code for the uniform/non uniform mesh; this can affect speed comparisons, as we expect having faster codes for uniform cubic splines. But as already said, we have not deeply looked at optimizations (neither in the uniform nor in the non uniform case). For non uniform mesh, we use an integer ratio $r = 32,\ a = 1.2,\ b = 1.6$, for the small drive amplitude, and $a = 0.375,\ b = 2.25$ for the standard case. Simulations are run on Hydra (computing centre of the Max Planck Society) and Helios Computational Simulation Centre, International Fusion Energy Research Centre of the ITER Broader Approach) supercomputers, with typical runs on 256 processors (16 nodes; each node having 16 threads).

3.1 Convergence study for the small drive case

On Figure 1, δ-$f = f - f_0$ distribution function is plotted at times $T = 500 + i500,\ i = 0, \ldots, 9$ and the 5 first ρ harmonics, that is the absolute values of the Fourier modes of $\rho = \int_{\mathbb{R}} f dv$, from mode $k = 1$ to mode $k = 5$. For this simulation, a *standard run* is used with the following numerical parameters: non uniform mesh, with $N_v = 16384$, $\Delta t = 0.5$ and 6th order Vlasov-Poisson splitting scheme. The run took 3453 seconds.
In order to study the convergence, we look at the diagnostic of the 5 first ρ harmonics and make a comparison with different numerical parameters. More precisely, we give comparisons with refined runs using the classical method (Figures 2,3) and the same method (Figures 4,5).
On Figure 2, we compare the standard run with a *uniform refined run*: uniform mesh, with $N_v = 262144$, and other same numerical parameters as the standard run. Note that the result is very similar, as here $N_{\text{fine}} = 258432$, for the standard run. The run took 54800 seconds, that is 16 times more than the standard run.
On Figure 3, we compare the standard run with a *Strang refined run*: Strang splitting, with $\Delta t = 0.0078125$ and other same numerical parameters as the standard run. The run took 72015 seconds, that is 21 times more than the standard run.
On Figure 4, we compare the standard run with a *time refined run*: $\Delta t = 0.25$, and other same numerical parameters as the standard run. The run took 6905 seconds, that is 2 times more than the standard run, which is expected.
On Figure 5, we compare the standard run with a *non uniform refined run*: $N_v = 65536$ and other same numerical parameters as the standard run. The run took 12589 seconds, that is 3.6 times more than the standard run.
We have also checked (not shown here) that taking $N_x = 1024$ instead of $N_x = 2048$ leads to results that are in the same range of convergence.

With all this plots, we can appreciate, how well we are converged with the standard run. Note that we gain here a factor $300 \simeq 16 \times 21$, with respect to the classical method; this factor may be decreased by considering optimized versions of the code, but should remain in the same order of magnitude.

3.2 Convergence study for the standard case

In the standard case, we are not able to obtain such good results, as the region of interest is bigger; we had also to use much smaller time steps; using bigger time steps lead to results that are qualitatively similar in the late time $T = 1000$ but differ with shifts of the delta-f distribution function and non match of the ρ harmonics, as already shown in [13]; we can however expect a better behaviour, if we fix the final time earlier, that is around $T = 400,\ 600$ where the KEEN wave is already formed.

On Figure 6, delta-f distribution function is plotted at times $T = 100 + i100,\ i = 0, \ldots, 9$ and the 5 first ρ harmonics, that is the absolute values of the Fourier modes of ρ, from mode $k = 1$ to mode $k = 5$. For this simulation, a *standard run* is used with the following numerical parameters: non uniform mesh, with $N_v = 16384$, $\Delta t = 0.00625$ and 6th order Vlasov-Poisson splitting scheme. The run took about 11 hours, that is 39600 seconds.

On Figure 7, we compare (for checking the accuracy in velocity) two runs with $\Delta t = 0.025$, the first one with $N_v = 16384$ and the second with $N_v = 32768$, and other parameters are similar than the standard run. The first run took 13799 seconds, and the second, 24959 seconds.

On Figure 8, we compare the standard run with a *time refined run*: $\Delta t = 0.0015625$, and other same numerical parameters as the standard run. The run took 69540 seconds on 1024 processors (64 nodes; each node having 16 threads).

On Figure 9, we compare the *time refined run* with a *refined run using Strang splitting*: $\Delta t = 0.001171875$, and other same numerical parameters as the standard run.

On Figure 10, we compare the *refined run using Strang splitting* with a less refined one: $\Delta t = 0.003125$, and other same numerical parameters as the refined run using Strang splitting.

We see here that convergence in time is quite difficult to achieve; a restart strategy should be added for having the possibility to make longer runs (typically more than 24 hours).

We also remark that Strang splitting leads to results with similar accuracy, for a given computational effort; however, if we look for a smaller final time, we can get better results with the new 6th order scheme (results not shown), taking larger time steps. A further study should be envisaged in order to better understand this phenomenon. For the moment, we expect that the solution is not so smooth and more complex in the standard case, as we can see it on the distribution function snapshots.

3.3 Small drive amplitude and different drive times

Finally, we give numerical results, by making vary the drive time $T_{\rm dr}$, in the case of the small drive amplitude $a_{\rm dr} = 0.00625$. We take the same numerical parameters than the standard run of the small drive amplitude case; the only difference is that we take the final time $T = 10000$ and we change $T_{\rm dr}$. On Figures 11 to 18 , delta-f distribution function is plotted at times $T = 1000 + i1000,\ i = 0, \ldots, 9$ and the 5 first ρ harmonics, that is the absolute values of the Fourier modes of ρ, from mode $k = 1$ to mode $k = 5$. The values of $T_{\rm dr}$ change successively: 100, 125, 150, 175, 200, 250, 300, 400. We observe forming and ill forming KEEN waves depending on the drive time. This a preliminary parameter study; further investigations will be pursued [3].

4 Conclusion

Further cross validations should be pursued, by using other non uniform methods, as developed in [18], for example. New numerical experiments by changing the physical parameters can then be continued and important physical diagnostics should be added and consolidated, for working with large meshes and huge number of processors; as already said, the extension to $2D \times 2D$ simulations is also envisaged. Of course, such simulations open also the door to design or test other new resolution techniques, that would use less complexity with similar numerical accuracy. It is also important to extend these techniques to the Vlasov-Maxwell setting and consider stimulated KEEN wave scattering, SKEENS and its interaction with SRS as well as to study KEEN-KEEN interactions and KEEN-EPW interactions. The later requires fine mesh solutions to encompass the entire region of velocity where the EPW phase velocity is and the KEEN wave phase velocity. This requires at least three times as wide a range in finely resolved v than was used in this paper.

References

1. B. Afeyan, M. Charbonneau-Lefort, K. Won, V. Savchenko, M. Shoucri,
The Generation of Self-Organization of Ponderomotively Driven Kinetic Electrostatic Electron Nonlinear (KEEN) Waves in High Energy Density Plasmas, Manuscript in preparation 2014.
2. B. Afeyan, K. Won, V. Savchenko, T. Johnston, A. Ghizzo, and P. Bertrand, *Kinetic Electrostatic Electron Nonlinear (KEEN) waves and their interactions rriven by the ponderomotive force of crossing laser beams.*, Proc. IFSA 2003, 213, 2003, and arXiv:1210.8105.
3. B. Afeyan, A. Dodhy, M. Mehrenberger, E. Sonnendrücker, *Long time evolution of KEEN waves excited with low levels of ponderomotive drive*, in preparation.
4. I. Bernstein, J. M. Greene, and M. Kruskal, *Exact nonlinear plasma oscillations*, Phys. Rev. 108, 546, 1957.
5. M. Brunetti, V. Grandgirard, O. Sauter, J. Vaclavik, L. Villard, *A semi-Lagrangian code for nonlinear global simulations of electrostatic drift-kinetic ITG modes*, Computer Physics Communications **163** (2004) pp. 1-21.
6. F. Casas, N. Crouseilles, E. Faou, M. Mehrenberger, *High-order splitting in time for the Vlasov-Poisson equation*, in preparation.
7. Y. Cheng, I. M. Gamba, P. J. Morrison, *Study of conservation and recurrence of Runge-Kutta discontinuous Galerkin schemes for Vlasov-Poisson systems*, J. Sci. Comput. **56** (2013), pp. 319-349.
8. C. Z. Cheng, G. Knorr, *The integration of the Vlasov equation in configuration space*, J. Comput. Phys. **22** (1976), pp. 330-351.
9. N. Crouseilles, M. Mehrenberger, E. Sonnendrücker, *Conservative semi-Lagrangian schemes for Vlasov equations*, J. Comput. Phys. **229** (2010), pp. 1927-1953.
10. J. L. Kline, B. Afeyan, W. A. Bertsche, N. A. Kurnit, D. S. Montgomery, R. P. Johnson, C. Niemann, *Demonstration of an optical mixing technique to drive Kinetic Electrostatic Electron Nonlinear waves in laser produced plasmas*, arXiv:1211.1437.
11. E. M. Lifshitz, L. P. Pitaevski, *Course of theoretical physics (Landau-Lifshits),* Vol. 10. Pergamon Press, Oxford, 1981. Translated from the Russian by J. B. Sykes et R. N. Franklin.
12. M. Mehrenberger, N. Crouseilles, E. Sonnendrücker, B. Afeyan, *High-order numerical methods for KEEN wave Vlasov-Poisson simulations,* Poster, PPPS, 16-21 june 2013, San Francisco.
13. M. Mehrenberger, C. Steiner, L. Marradi, N. Crouseilles, E. Sonnendrücker, B. Afeyan, *Vlasov on GPU (VOG project)*, ESAIM: Proc. Vol. 43, December 2013, CEMRACS 2012, 37–58.
14. D. S. Montgomery, R. J. Focia, H. A. Rose, D. A. Russell, J. A. Cobble, J. C. Fernandez, R. P. Johnson, *Observation of stimulated electron-acoustic-wave scattering*, Phys. Rev. Lett., **87(15)** (2001), pp. 5001-5004.
15. D. S. Montgomery, J. A. Cobble, J. C. Fernandez, R. J. Focia, R. P. Johnson, R. P. Renard-LeGalloudec, H. A. Rose, D. A. Russell, *Recent Trident single hot spot experiments: Evidence for kinetic effects, and observation of Langmuir decay instability cascade*, Phys. Plasmas **9** (2002), pp. 2311–2320.
16. http://selalib.gforge.inria.fr/
17. M. Shoucri, B. Afeyan, *Stimulated Raman scattering with a relativistic Vlasov- Maxwell code: cascades of nonstationary nonlinear kinetic interactions,* Computational and Numerical Simulations, Prof. Jan Awrejcewicz (Ed.), ISBN: 978-953-51-1220-4, InTech Publication 2014. DOI: 10.5772/57476.
18. C. Steiner, M. Mehrenberger, *A semi-Lagrangian discontinuous Galerkin scheme for Vlasov-Poisson equation*, Vlasovia 2013, poster session.

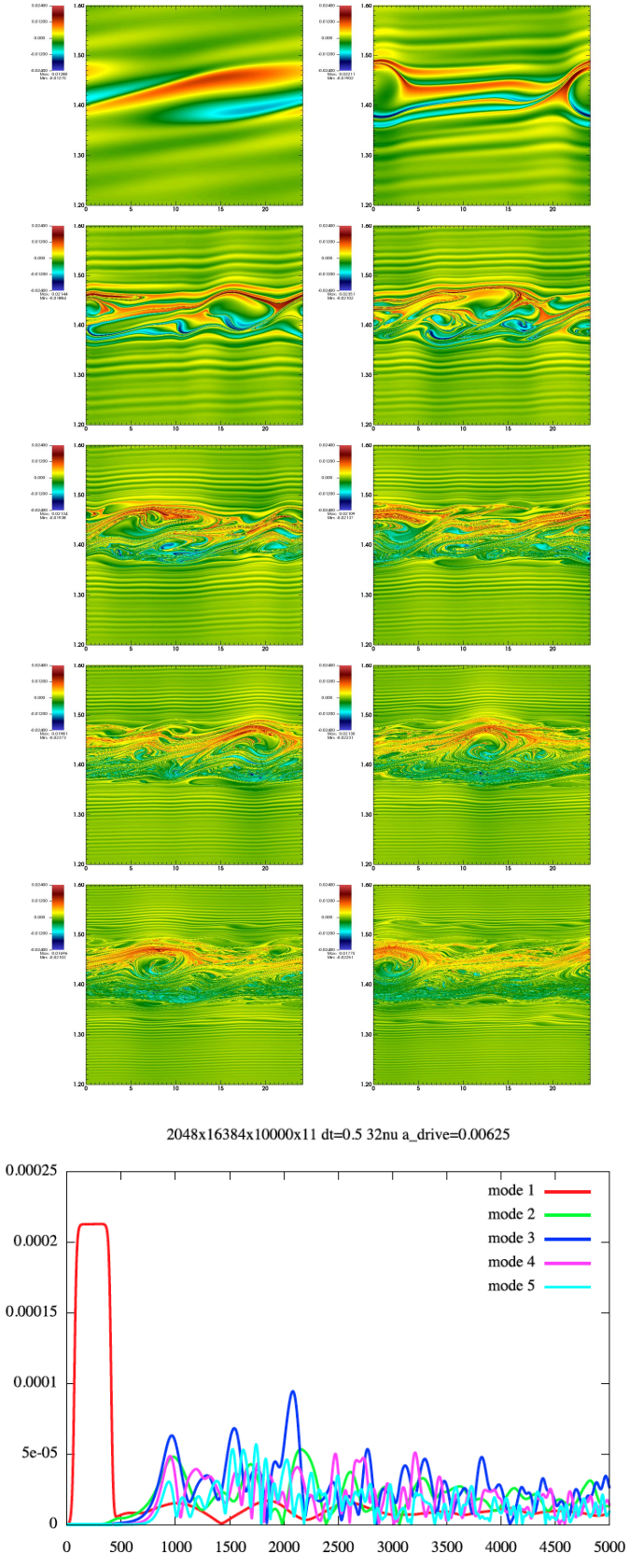

Fig. 1. Small drive amplitude case

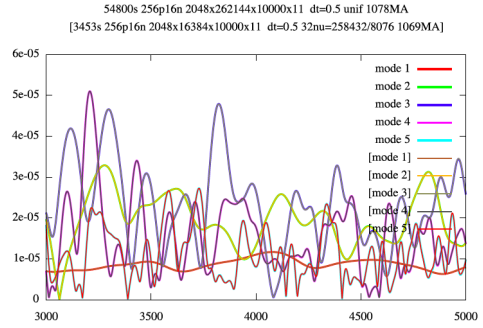

Fig. 2. Small drive: uniform vs [non-uniform]

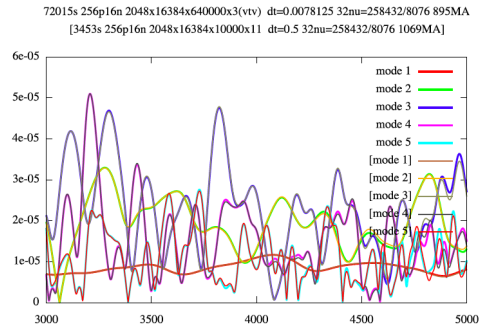

Fig. 3. Small drive: Strang vs [6th order scheme]

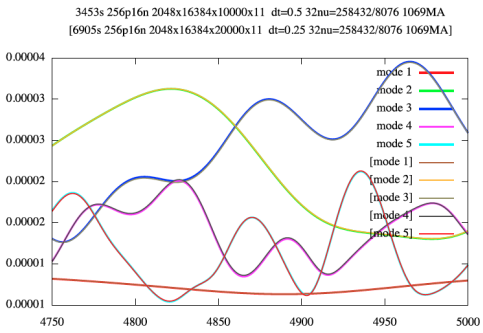

Fig. 4. Small drive: $\Delta t = 0.5$ vs $[\Delta t = 0.25]$

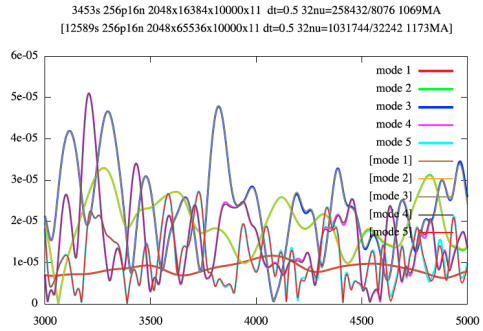

Fig. 5. Small drive: $N_v = 16384$ vs $[N_v = 65536]$

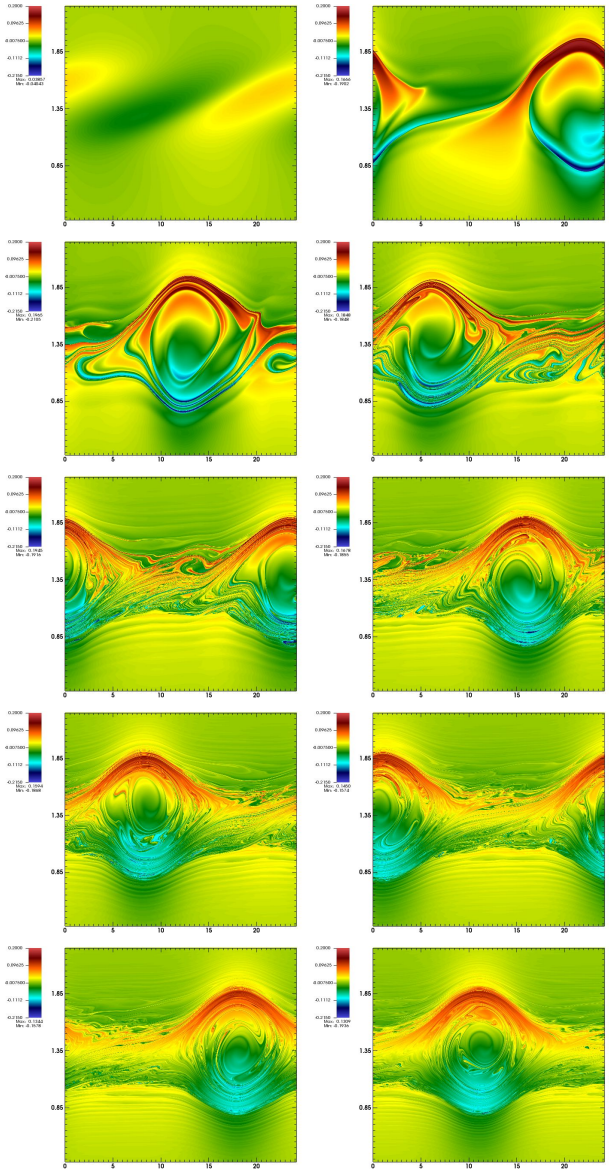

2048x16384x160000x11 dt=0.00625 32nu a_drive=0.2 11h hydra

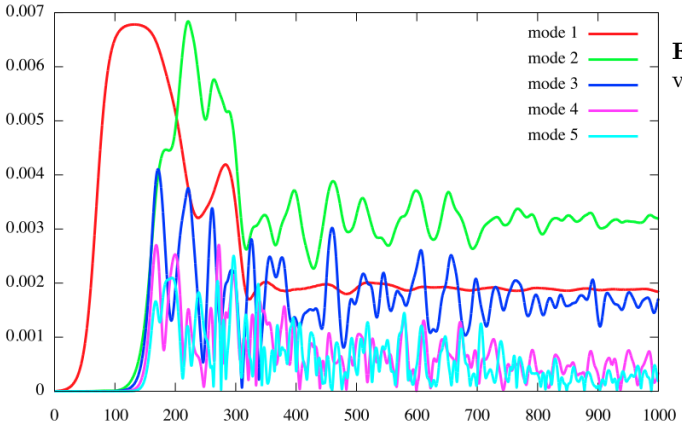

Fig. 6. Standard case

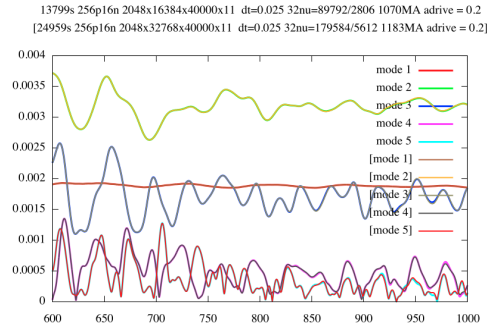

Fig. 7. Standard case: $\Delta t = 0.025$, $N_v = 16384$, [32768]

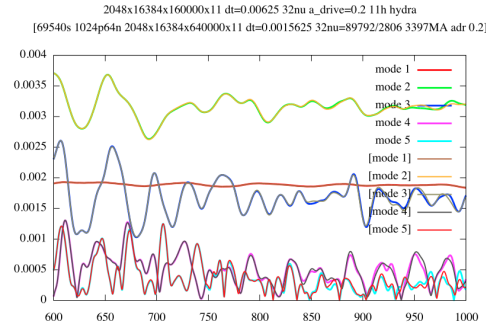

Fig. 8. Standard case: $\Delta t = 0.00625$ vs. [$\Delta t = 0.0015625$]

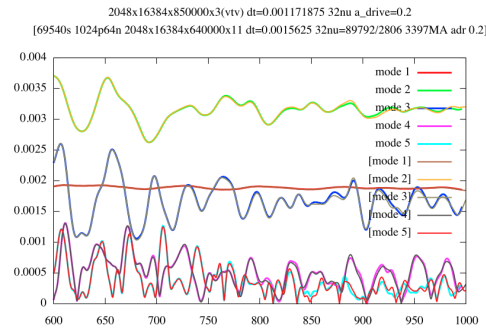

Fig. 9. Standard case: $\Delta t = 0.001171875$, Strang, vs. [$\Delta t = 0.0015625$, 6th order scheme]

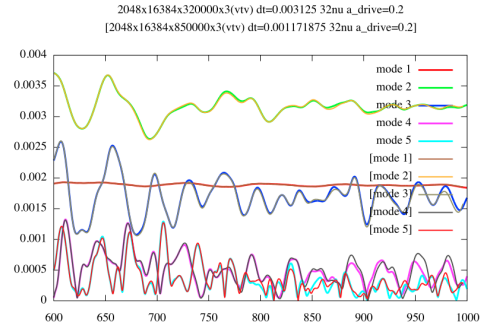

Fig. 10. Standard case: Strang, $\Delta t = 0.003125$, [0.001171875]

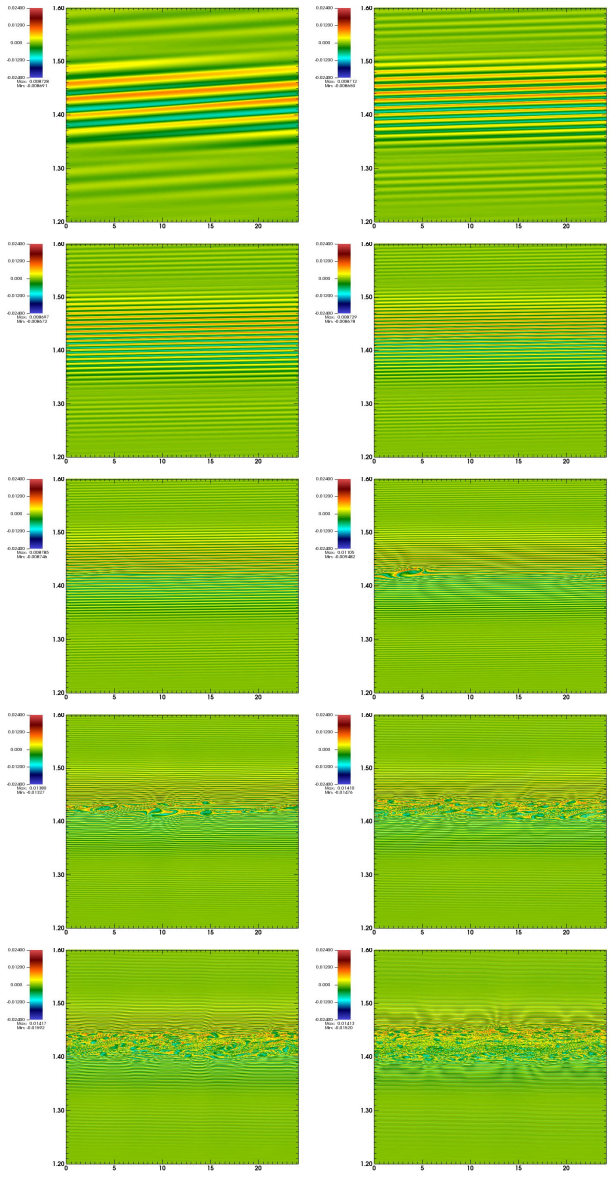

2048x16384x20000x11 dt=0.5 32nu a_drive=0.00625 tflat 100

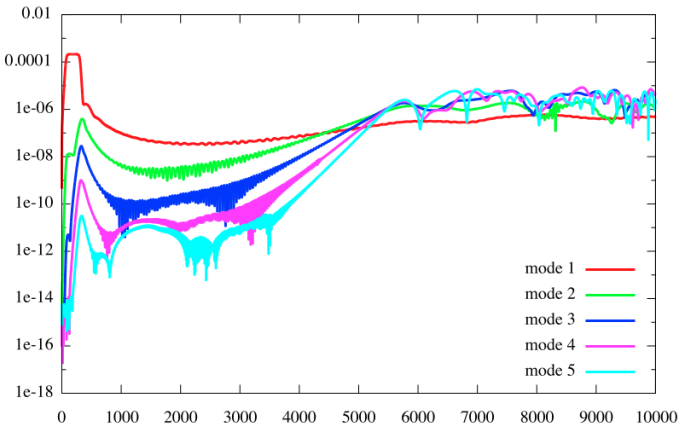

Fig. 11. $a_{\rm dr} = 0.00625$ and $T_{\rm dr} = 100$

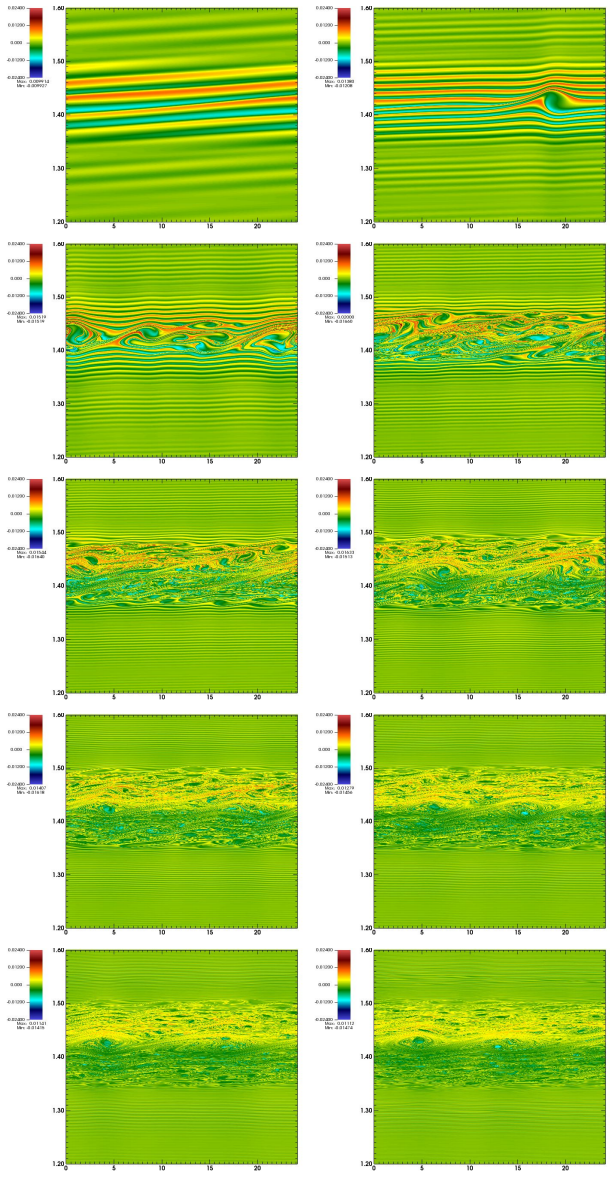

2048x16384x20000x11 dt=0.5 32nu a_drive=0.00625 tflat 125

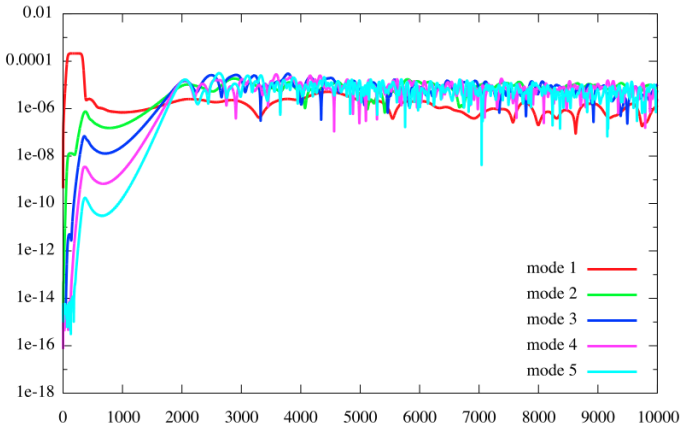

Fig. 12. $a_{\rm dr} = 0.00625$ and $T_{\rm dr} = 125$

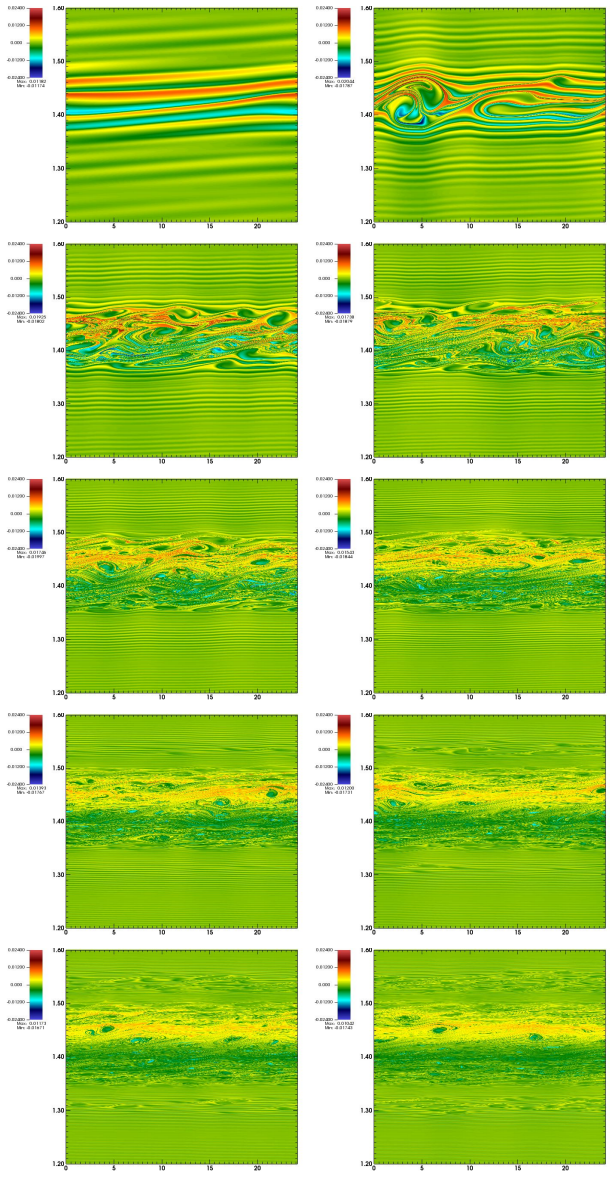

2048x16384x20000x11 dt=0.5 32nu a_drive=0.00625 tflat 150

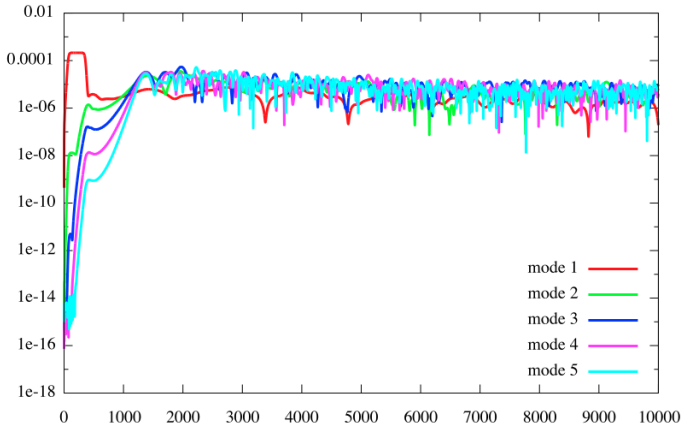

Fig. 13. $a_{\rm dr} = 0.00625$ and $T_{\rm dr} = 150$

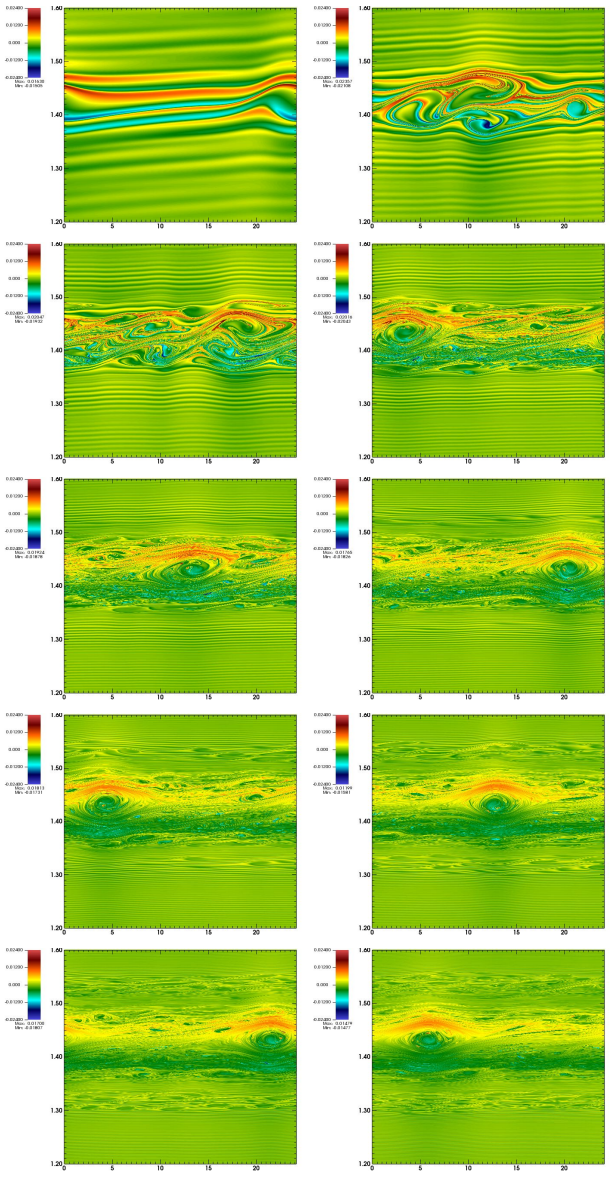

2048x16384x20000x11 dt=0.5 32nu a_drive=0.00625 tflat 175

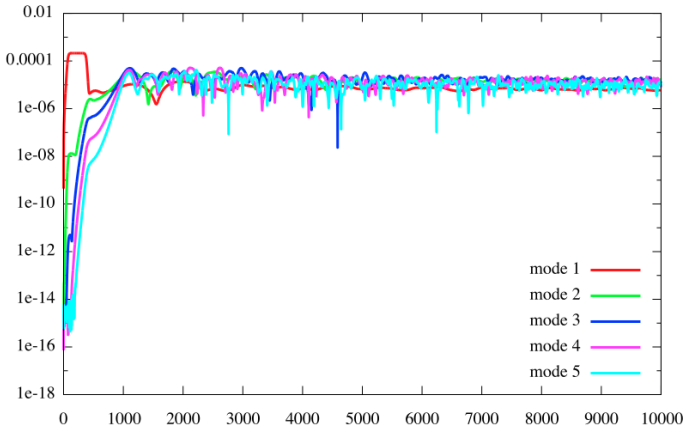

Fig. 14. $a_{\rm dr} = 0.00625$ and $T_{\rm dr} = 175$

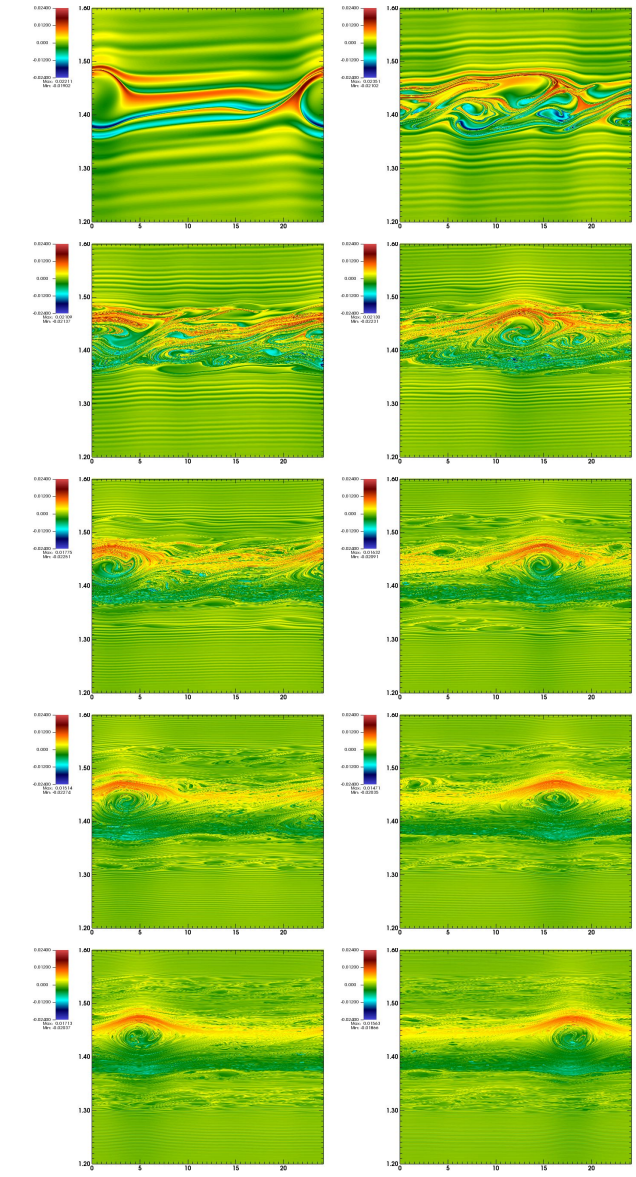

2048x16384x20000x11 dt=0.5 32nu a_drive=0.00625

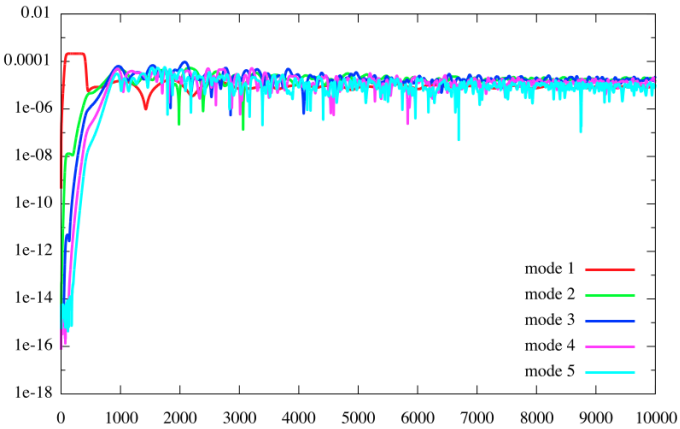

Fig. 15. $a_{\rm dr} = 0.00625$ and $T_{\rm dr} = 200$

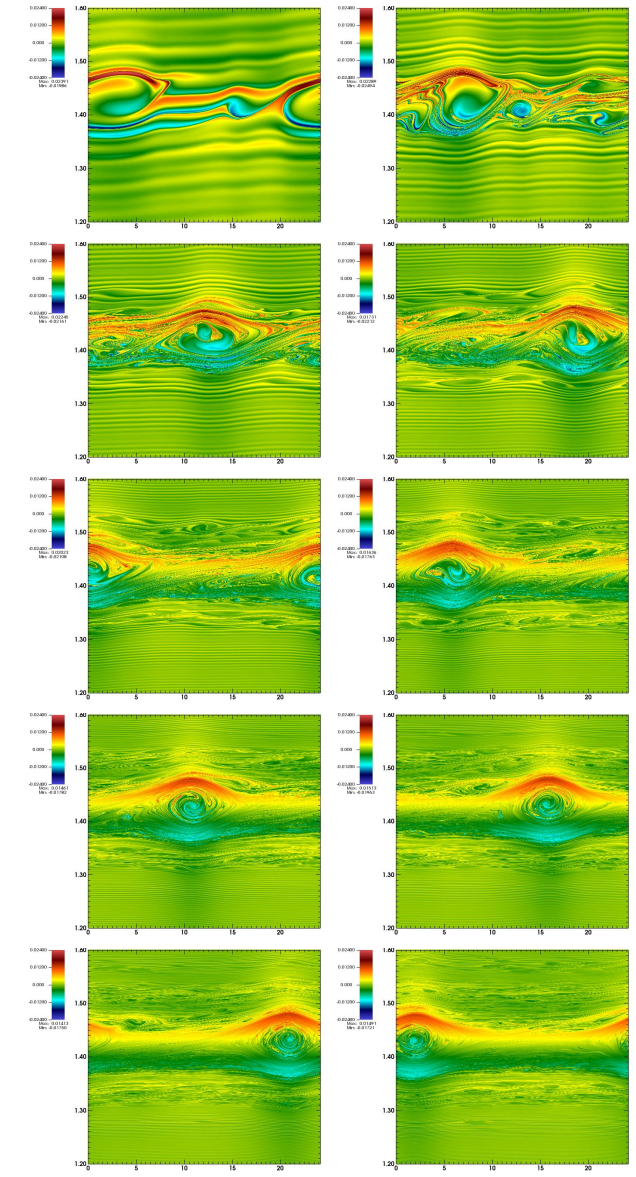

2048x16384x20000x11 dt=0.5 32nu a_drive=0.00625 tflat 250

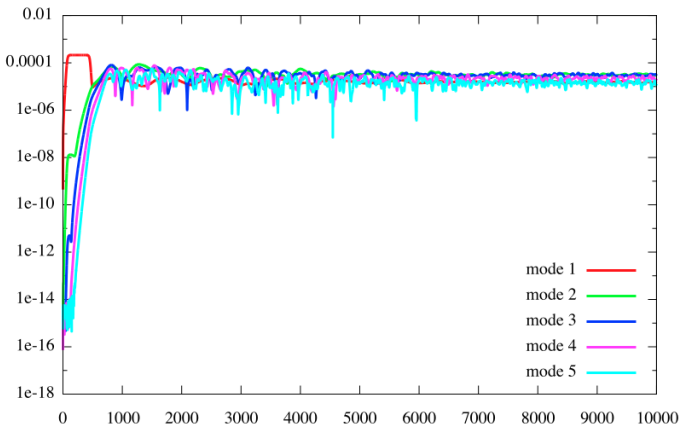

Fig. 16. $a_{\rm dr} = 0.00625$ and $T_{\rm dr} = 250$

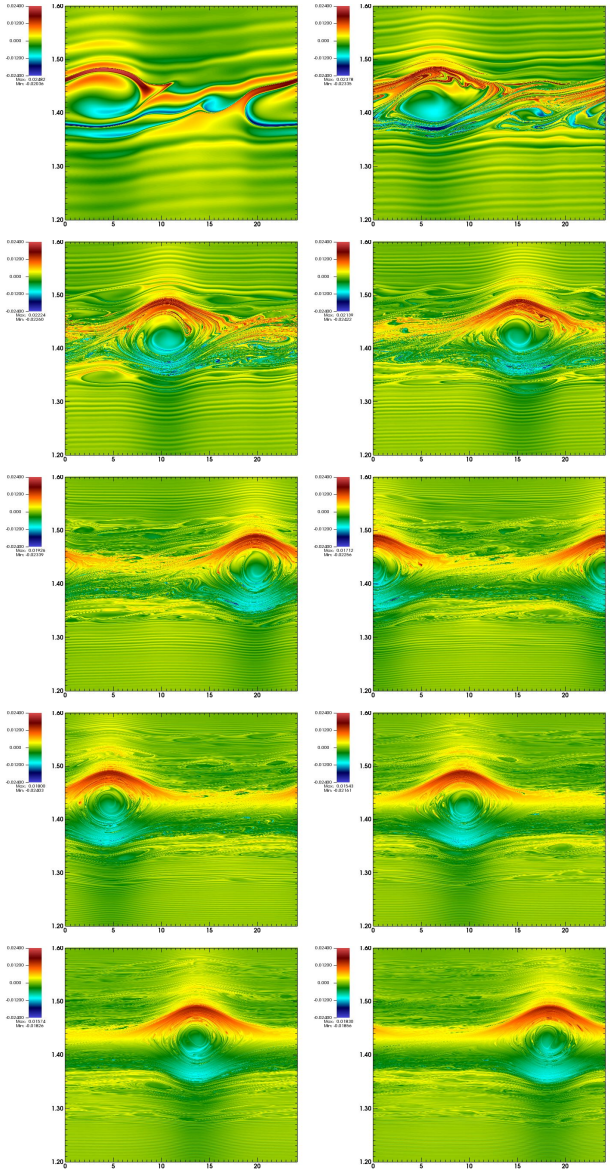

2048x16384x20000x11 dt=0.5 32nu a_drive=0.00625 tflat 300

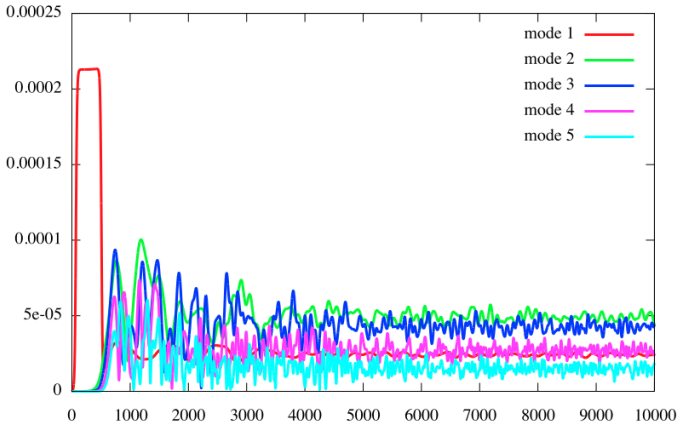

Fig. 17. $a_{\rm dr} = 0.00625$ and $T_{\rm dr} = 300$

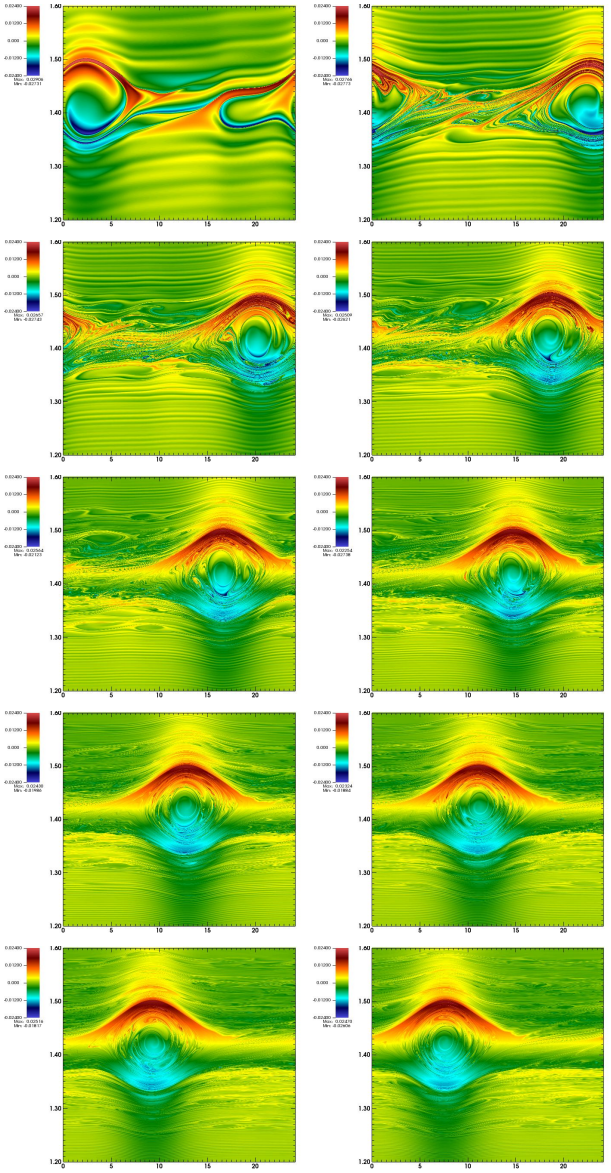

2048x16384x20000x11 dt=0.5 32nu a_drive=0.00625 tflat 400

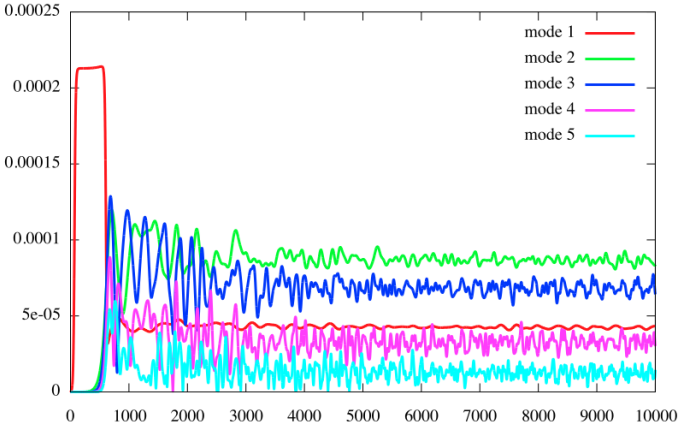

Fig. 18. $a_{\rm dr} = 0.00625$ and $T_{\rm dr} = 400$